

Freak waves with deep trough in the sea

(Three reasons for freak wave generation in non-uniform current)

Lavrenov I.V.(1), Porubov A.V.(2)

1) Arctic and Antarctic Research Institute, St.Petersburg, Russia

<lavren@aari.nw.ru>

2) A.F. Ioffe Physical Technical Institute, St.Petersburg, Russia

Introduction

During last years considerable attention has been paid to the freak wave investigation as the phenomenon producing dangerous impact on ships and oil platforms in seas. According to the modern definition, this phenomenon is a wave with height being larger than 2.2 times of significant wave height value. In fact, as soon as wind wave height distribution is approximated by the Relay distribution with sufficient accuracy, it allows getting any wave height value with appropriate probability. It means that the wave height with the value larger than 2.2 times of significant value can be found in any wave record. It becomes obvious that in case of a freak wave, as a dangerous natural phenomenon, such definition is not sufficient.

It should be noted that originally the term ‘freak waves’ (or abnormal waves, exceptional waves, killer waves, freak waves, cape roller and rogue waves) pertains to individual asymmetric waves with a crest of an extremely high slope, in front of which there appears a longer and deeper trough than compared with ordinary wind waves. This trough looks like a hole in the sea. It is rather difficult to observe a hole at some distance from a ship. However, the total height of such waves can reach 15-20 m and more, sometimes in a relatively calm sea. Waves often appear suddenly. That is why it is practically impossible for a ship’s crew to take any precaution measures.

Abnormal waves are observed frequently in different regions of the world ocean, where there are strong currents: for example, Gulfstream, Kuroshio and others. Extremely large waves are observed near the southeastern shore of South Africa in the Agulhas current between East London and Durban (Fig. 1). That is why the region is considered to be very dangerous. A list of cases when abnormal waves were observed up to 1973 is presented by captain Mallory (Mallory, 1974), along with an analysis of the corresponding atmospheric and oceanographic conditions, which were responsible to a great extent for the appearance of the abnormal waves. In his article, captain Mallory showed 11 cases of catastrophic ship collisions with abnormal waves in the region (Fig. 1.). The conditions mainly come down to the conjunction of the southwesterly waves with the passage of an atmospheric cold front. In fact, abnormal waves appeared here more often and the consequences of their action were less dramatic. It can be explained by weather conditions of the area when ships had to slow down their speed and diminish the effect of the wave action.

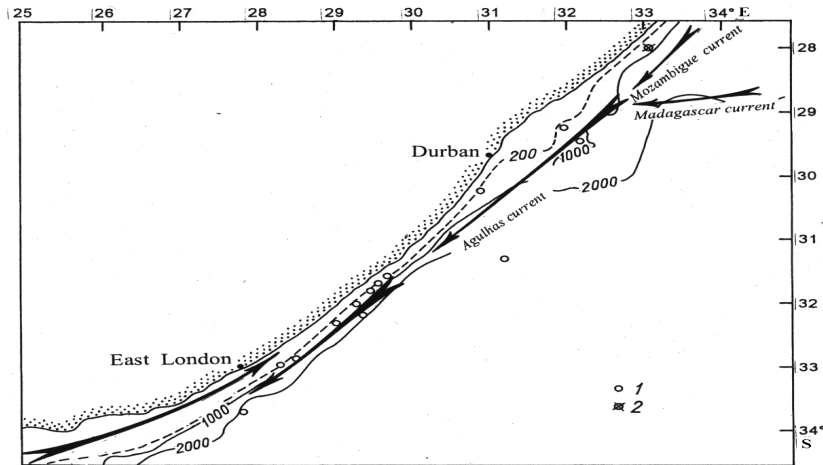


Fig. 1. Map of the Southeast Coast (South Africa).
 1 – location abnormal wave accident;
 2 – Location of the "Taganrogsky zaliv" tanker-refrigerator

On April 27, 1985 at 01.01 p.m. ship time (11.01 a.m. GMT), the Soviet tanker-refrigerator "Taganrogsky Zaliv"¹ was subjected to the abnormal wave (point of accident is denoted by a circle with a cross in Fig. 1.). As a result, a sailor working on a fore deck was mortally wounded and washed overboard.

That time one of the authors of this paper was invited as a wind wave expert to take part in the work of the Commission of the Crimean Transport Prosecuting Office, examining the incident (Lavrenov, 1985a). As a result of the Commission's investigations, a number of peculiar details concerning abnormal wave generation were revealed. They were used later in mathematical modeling of this phenomenon.

On date under discussion, the "Taganrogsky Zaliv" tanker-refrigerator was sailing from the Indian Ocean to the Southeast Atlantic. The possibility of encountering a weather storm is high enough near the Cape of Good Hope. That is why the ship was prepared for sailing in stormy weather. The north-north east wind was blowing at a speed of 7 m s^{-1} . At 5 a.m., it changed its direction to south-south west with the same force. From the previous day the atmospheric pressure was diminishing until the wind changed direction, after that it began increasing. At 8.00 a.m., the wind became stronger and at 11.00 a.m. it reached 15 m s^{-1} . After 12.00, the wind speed diminished to 12 m s^{-1} . Sea wind became calmer. The wind force did not change during the next three hours. Wave height did not exceed 5m and the length was 40-45 m. The weather conditions were suitable for fulfilling deck reparation works. The location of the ship is shown by cross in Fig. 1 (Lavrenov, 1985). About 13.00 the front part of the ship suddenly dipped, and the crest of a very large wave appeared close to the foredeck. It was 5-6 m higher over the foredeck. The wave crest fell down on the ship. One of the seamen was killed and washed overboard. All attempts to save him were in vain. Nobody was able to foresee the appearance of such a wave. When the ship went down, riding on the wave, and its frontal part was stuck into water, nobody felt the wave's impact. The wave easily rolled over the foredeck, covering it with more than two meters of water (see Fig.2). The length of the wave crest was not more than 20 m. Accident of freak wave impact of the ship is presented in Fig.2 according to ship's crew description.

¹ "Taganrogsky zaliv" is a ship of the unrestricted sailing radius. The vessel length is 164.5 m, the largest width is 22 m, the displacement during accident was 15 000 ton, the board height above water was 7 m.

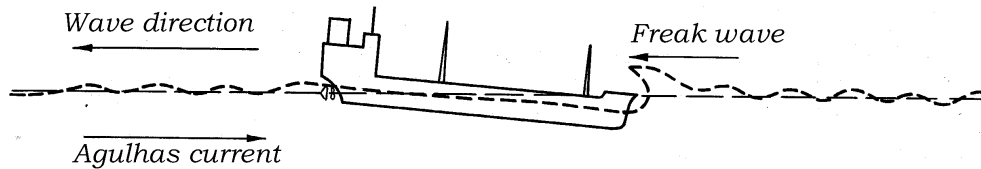


Figure 2: Rogue (freak) wave attack on the ship.

According to the ship's crew description, the unusual wave looked like a deep hole in the sea, which appeared so suddenly in front of the ship that it was practically impossible to make any precaution measures to avoid ship's sliding down into deep wave trough.

Recently another abnormal waves with deep trough were registered in the ocean. Such a wave was observed near the South Africa coastal zone, where the ocean depth was 70 m [6], See Fig. 3. It looks like the usual envelope wave but for the part with deep trough marked by an arrow in Fig.3. Its magnitude A is equal to $A = 11$ m while the neighboring crests are not higher than 6 m. The speed of the wind was about $U0 = 30$ m/sec. In this case the velocity of the wind turns out about the velocity of the linear surface waves in limited depth \sqrt{gH} .

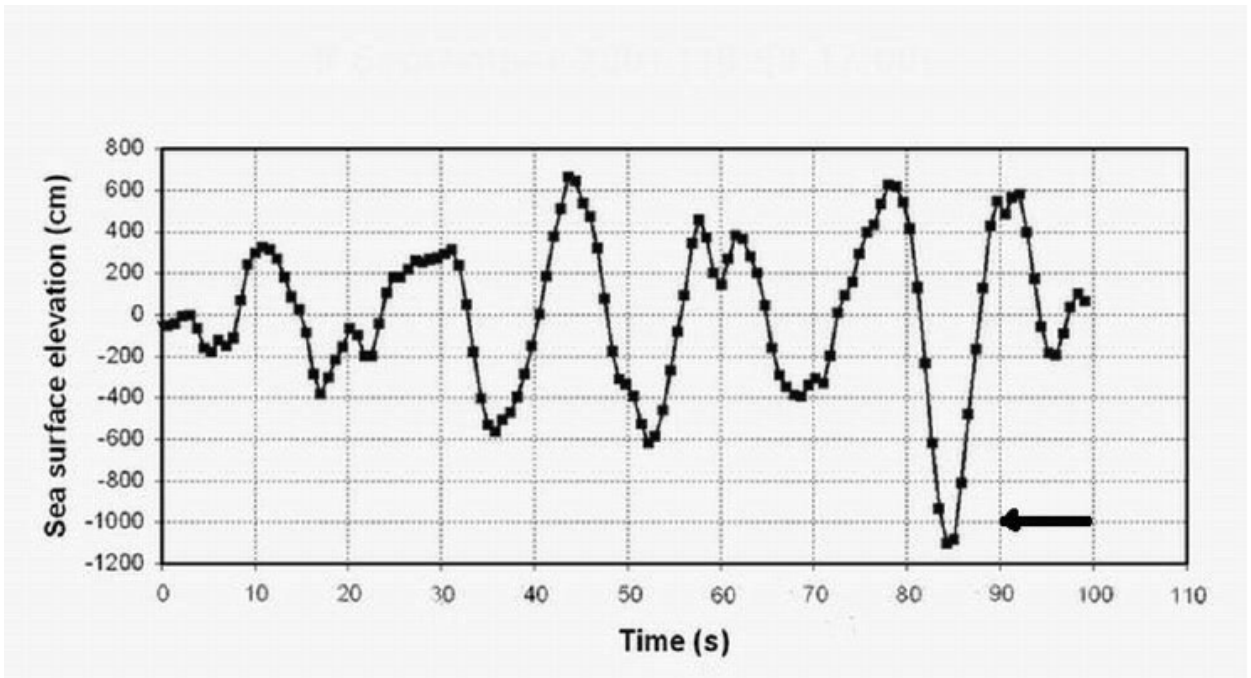


Fig.3. Observation of a hole near the South Africa coast. Abnormal hole is marked by an arrow.

Nowadays there are a lot of different results devoted to the freak wave investigation. Detailed result analysis is published by Kharif and E. Pelinovsky (2003). It should be noted that the main attention in almost all papers is paid to the study of generation wave with a large crest. At the same time there is lack of results devoted to the generation of wave with deep trough (WWDT) in the sea.

From the linear theory point of view the probability observing wave with large crest is the same as for wave with deep trough. On the other hand, from the non-linear surface wave theory (at least for Stocks wave theory or solitary wave in shallow water) the value of crest is larger than value of trough depending on wave steepness.

There is a question what kind of physical mechanisms can be responsible for the wave with deep trough generation (WWDT) in the sea.

Starting from the water wave theory it is hardly possible to suppose obtaining a solution for WWDT. However, other mechanisms of the freak wave generation can be applied for explanation of the WWDT generation in the sea. So, the following mechanisms should be mentioned:

- Wave transformation in non-uniform current (Lavrenov, 1985, 1998);
- Dispersion focusing (Kharif, Pelinovsky, 2003) as soon as it can be based on linear theory;
- Non-linear modulation (Osborne et.al, 2002) based on Schrödinger equation for wave envelop;
- Wave refraction due to uneven bottom (Kharif, Pelinovsky, 2003);
- Spatial non-uniform and/or temporal non-steady wind field (Lavrenov, 1985, 1998);

In the present paper, main attention will be paid to the problem of the wave transformation in non-uniform current, which can produce WWDT. In turn, there are at least three reasons for freak wave generation in non-uniform current. They can be mentioned as follows:

- Wave energy amplification due to wave-current interaction;
- Wave height amplification around caustic due to refraction wave in non-uniform current;
- Non-linear wave interaction in shallow water due to their intersection described by KP equation;

1. Wave energy amplification due to wave-current interaction

The Agulhas current is a necessary condition for freak wave generation. A large wave appearance in the Agulhas current can be explained by a local wave pattern generated by wave reflection from the current. The abnormal waves are typically observed on the oceanic surface, where the depth approximately coincides with a 200-m isobath. The latter passes parallelly to the coastline. It is the boundary of the continental shelf, where the depth increases sharply to 3-4 km (see Fig. 1). The sharp depth variation at the continental shelf margin results in the maximum values of the Agulhas current, having a jet profile directed parallel to the shoreline. The transversal profile of the Agulhas current velocity distribution is not changed much along its entire length from the Mozambique and South Madagascar current confluence at the latitude 30 degree South (see Fig.1). The typical horizontal profile of the current velocity distribution in the transversal direction (Schumann, 1976) is presented in Fig. 4. The axis Ox of the co-ordinate system is chosen along the current velocity direction, and the axis Oy is in the perpendicular one. A transversal profile of the current velocity $V = \{V_x(y), 0\}$ in this area can be quite accurately approximated using the relation:

$$V_x = \frac{b_1}{1+b_2y^2}, \quad (1.1)$$

Where $b_1=2.2 \text{ m s}^{-1}$; $b_2=6.25 \cdot 10^{-10} \text{ m}^{-2}$ at $y<0$; $b_2=10^{-8} \text{ m}^{-2}$ at $y>0$.

The current velocity distribution (1.1) is assumed to be valid at $x<0$ in the chosen co-ordinate system. The point $\{x=0, y=0\}$ is assumed to be correspondent to the current velocity midstream at the point with co-ordinates $\{27^\circ \text{ E}, 34^\circ \text{ S}\}$.

The Agulhas current is diverged in a fan-shaped manner at more southern latitudes, becoming weaker. It can be assumed that in the case $x>0$, the horizontal current velocity components $V = \{V_x(x, y), V_y(x, y)\}$, satisfying the water flux continuity equation, are approximated by the equations:

$$V_x = \frac{b_1}{(1+b_2y^2)(1+b_3x^2)}; \quad V_y = \frac{2b_1b_3x}{(1+b_3x^2)\sqrt{b_2}} \arctan(\sqrt{b_2} y), \quad (1.2)$$

where $b_3=0.6 \cdot 10^{-11} \text{ m}^{-2}$.

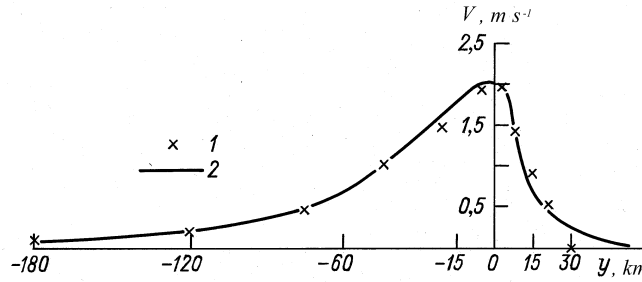


Fig. 1.4. Distribution of horizontal current velocity in transversal direction. 1 – velocity values according to Schumann (1976); 2 – approximation (1).

The swell propagation from southern latitudes, with actually no currents, towards the increasing Agulhas current should be considered. The geometric optics approximation can be applied in this case, because typical horizontal scales of current velocity variations exceed significantly the horizontal wave dimensions. At greater distance from the investigated area (see Fig.1), the initial spectrum $S_0(\omega, \beta_0)$ is assumed to be prescribed at $x > 1.5 \cdot 10^6 \text{ m}$, where the current speed can be neglected: $\sqrt{V_x^2 + V_y^2} \approx 0$. The spectrum can be described with the help of the swell spectrum approximation [Lavrenov, 2003] with $n=5$, $\omega_{\max} = 0.5 \text{ rad s}^{-1}$. It should be noted that the initial value of the angle β_0 included in $S_0(\omega, \beta_0)$ is a function of the values ω , β and the co-ordinates $\{x, y\}$.

In order to find β_0 , it is necessary to solve a set of the Hamilton equations, which can be written using new variables:

$$\begin{aligned} \frac{dy}{dx} &= \frac{V_y + \frac{1}{2} f \sin(\beta)}{V_x - \frac{1}{2} f \cos(\beta)}; \\ \frac{d\beta}{dx} &= \frac{\sin(2\beta) \frac{\partial V_x}{\partial x} - \sin^2(\beta) \frac{\partial V_y}{\partial x} + \cos^2(\beta) \frac{\partial V_x}{\partial y}}{V - \frac{1}{2} f \cos(\beta)}; \\ \frac{dt}{dx} &= \frac{1}{V - \frac{1}{2} f \cos(\beta)}, \end{aligned} \quad (1.3)$$

$$\text{where } f = \frac{1}{2} \frac{g}{\omega} \left\{ 1 + \left[4 - \frac{\sqrt{V_x^2 + V_y^2}}{g} \omega \cos \left(\beta + \arcsin \left(\frac{V_y}{\sqrt{V_x^2 + V_y^2}} \right) \right) \right] \right\}.$$

The Runge-Kutta method for a discrete set of the frequencies ω_i (from $\omega_1=0.37 \text{ rad s}^{-1}$ to $\omega_{12}=0.981 \text{ rad s}^{-1}$) and the angles β_j (from -75 to 75° with a step of 15°) the values β_{0j} are obtained. They correspond to the rays arriving to the given points $\{x=0, y=y_n\}$ from the region with practically no current $x > 1.5 \cdot 10^6 \text{ m}$.

Some most typical rays $y = y(x, \omega, \beta)$ arriving to the point $\{x=0, y=0\}$ are depicted in Fig. 5. They are characterized by oscillations relative to the axis Ox . The oscillation frequencies are increased with rays approaching the intense current area. A peculiar wave channel (i.e. a waveguide) appears in the current with the wave rays being alternatively reflected from one or other caustics situated on different sides of the current midstream.

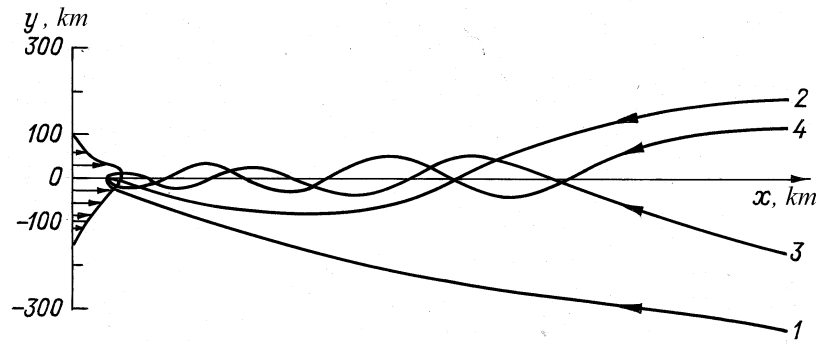


Fig. 5. Wave rays in jet current arriving to given point with frequency ω : 1 – 0.20 rad s^{-1} ; 2 – 0.38 rad s^{-1} (at angle $\beta_0 = -30^\circ$); 3 – 0.76 rad s^{-1} ; 4 – 0.93 rad s^{-1} (at angle $\beta_0 = 30^\circ$).

The wave spectrum in the current $S(\omega, \beta_j, y_n)$ is obtained at $x=0$ as a result of numerical simulation of the equations (1.3), using the spectral solution of the energy balance equation [Lavrenov, 2003]

$$S(\omega, \phi, U(y)) = \frac{16}{(1 + \sqrt{1 - 4U\omega/g \cos \phi})^4} \frac{S_0(\omega, \phi_0)}{\sqrt{1 - 4U\omega/g \cos \phi}} \quad (1.4)$$

. In order to obtain the total wave energy, the spectrum is integrated numerically over the frequency ω and the angle β . The estimation results (see Fig. 6) are obtained for the relative mean wave height h/h_0 in the current (where h_0 is the initial wave height without any current), whereas values of the co-ordinate y are plotted along the horizontal axis. The value h/h_0 maximum equal to 2.19 is estimated to be in the midstream. The ratio h/h_0 is sharply decreased along the distance to the shoreline. A relative excess of the wave height is not greater than 10 per cent at a distance of $y = 19 \cdot 10^3 \text{ m}$ from the maximum current velocity line. Seaward to the midstream, the relative height h/h_0 is decreased to a lesser extent with a ten-percent wave height excess, occurring at $y = -70 \text{ km}$. But a reversed case (i.e., $h < h_0$) is even observed at $|y| > 90 \text{ km}$. The probability of observing abnormal waves is much less in going towards the shore at some distance from the line of maximum velocity with 200 m isobath, than going the same distance from the maximum velocity current in the direction to the open sea.

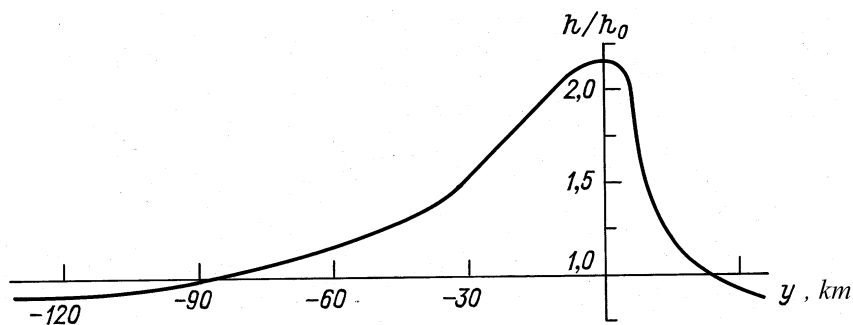


Fig. 6. Distribution of relative mean wave height across current.

Thus, the obtained results indicate that the peculiar velocity distribution of the Agulhas current induces refraction of the southwest swell propagating over a wide area of the southwestern Indian Ocean. It leads to that the swell turns towards the current velocity maximum. The swell is trapped, intensified by the countercurrent and localized in the neighborhood of the maximum velocity, propagating along the southeast coast of South Africa. As a result, there is a significant

concentration of the wave energy density, i.e. a focusing takes place in the given area resulting in abnormal wave generation.

2. Wave height amplification around caustic due to refraction wave in non-uniform current

Spectral solution obtained above provides estimation of the mean wave height spatial distribution. This solution is space averaged. The wave phase is omitted. That is why it does not describe waveform as it is. In order to solve this problem the diffraction approach can be applied for wind wave transformation in cross velocity shear current.

The current velocity V is assumed to be directed along the axis Oy with its changes along the coordinate x : $V = \{ 0; V_y(x) \}$. The depth $H = H(x)$ is also changed along this direction (see Fig. 7). Such situation can appear, for example, in the coastal zone with a along shore current or in Agulhas current.

The equation for the wave packet propagation can be written in the following form:

$$\frac{dx}{dt} = C_{gx} = C_g \cos(\beta); \quad \frac{dy}{dt} = C_{gy} = C_g \sin(\beta) + V_y; \quad (2.1)$$

$$\frac{dk_x}{dt} = \frac{1}{2} \sqrt{\frac{gk}{\text{th}(kH)}} \frac{1}{\text{ch}^2(kH)} \frac{dH}{dx} + k_y \frac{\partial V}{\partial x}; \quad \frac{dk_y}{dt} = 0. \quad (2.2)$$

As it can be seen from the problem formulation, the coordinate y is cyclic. The component k_y of the wave vector k remains constant along a wave packet propagation trajectory. It can be written as:

$$k_y = k \sin(\beta) = k_0 \sin(\beta_0). \quad (2.3)$$

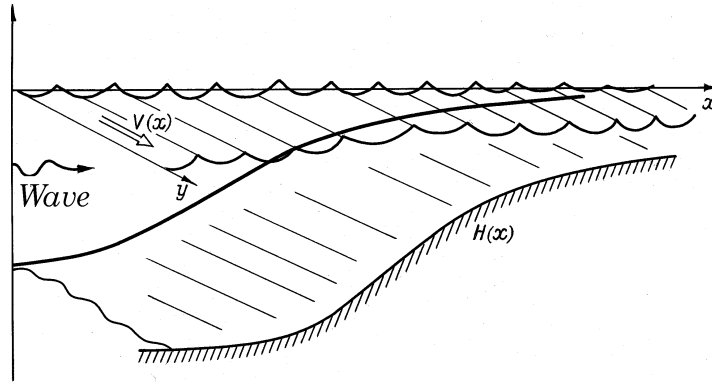


Fig. 2.1 Wave transformation in a shear horizontally non-uniform current.

Trajectories of wave packet propagation against current velocity profile and depth background for different quadrants are presented in Fig. 2.2 .

In order to estimate the wave field around caustic precisely it is necessary to fulfill more accurate calculations than it is made for usual spectral problem solution. For this purpose a modified traditional scheme of the VKB approximation can be applied. In order to do it the Maslov method (Maslov&Fedoryuk, 1976), describing the uniform wave field asymptotic in entire space can be used.

The application of the geometrical optics method leads to the amplitude value singularity in the caustic. However, in case the wave field is described by the integral representation the wave amplitude is finite around caustic. The Fourier integral is proposed to be used as a such representation. Integration is made over the wave vector component k_x , in which direction the wave medium properties are changed (for example, along the axis Ox). In other words, describing the wave field one proceeds from the spatial coordinates $\{x_1 = x, x_2 = y\}$ to the mixed spatial-momentum representation $\{k_1 = k_x, x_2 = y\}$. The wave vector component, directed along the axis Oy is constant, i.e. $k_y = k_{y0}$. The frequency ω is persevered along the ray as well:

$$\omega = F(k_x, k_{y0}, x) = \text{const}. \quad (2.4)$$

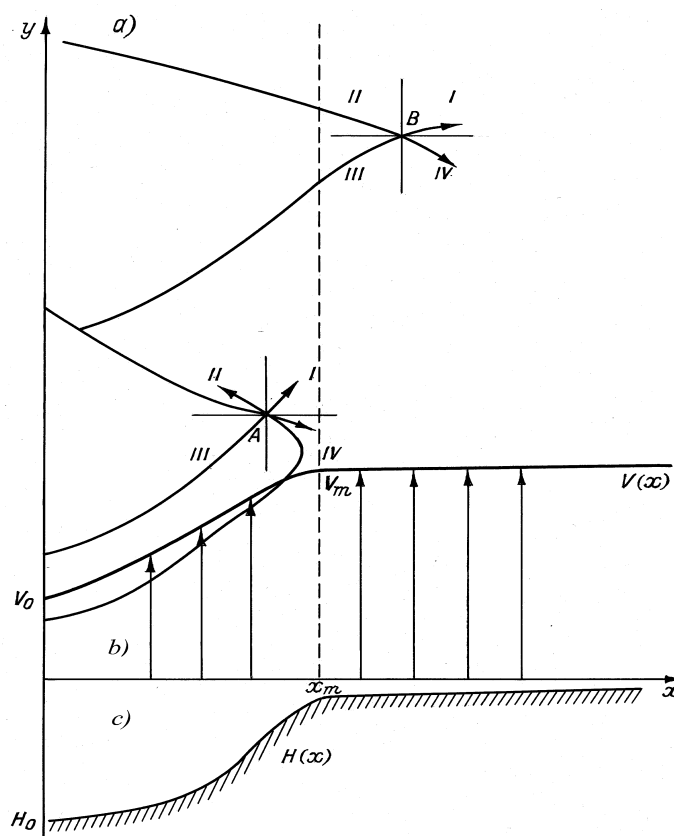


Fig. 2.2a,b,c. Trajectories of wave packet propagation against current velocity profile and depth background for different quadrants at points A and B (a); (b) – current velocity profile $V(x)$; (c) – depth change profile $H(x)$.

As it follows from the equations (2.1)-(2.2), the trajectory of the wave packet propagation can be parametrically presented in the following form:

$$\int_{x_0}^x C_{gx}^{-1} dx = t - t_0; \quad y = y_0 + \int_0^t C_{gy} dt, \quad (2.5)$$

Where the initial data are prescribed as $x|_{t=t_0} = x_0$; $y|_{t=t_0} = y_0$; $k_x|_{t=t_0} = k_{x0}$; $k_y|_{t=t_0} = k_{y0}$. The wave amplitude at the initial moment $a(x, y, t)|_{t=t_0} = a_0$ is also considered to be known.

According to the Maslov method scheme, the wave integral presentation can be written as:

$$\eta(x, y, t) = \frac{1}{\sqrt{2\pi}} \int a_0 \sqrt{\frac{\sigma}{\sigma_0} \left(\frac{\partial(k_x, y)}{\partial(x_0, y_0)} \right)^{-1}} \exp\{i [k_x(x - \tilde{x}) + \psi(\tilde{x})]\} dk_x, \quad (2.6)$$

Where the wave number k_x is the integration variable; \tilde{x} is the function of k_x , obtained from the equation (2.4) x ; $\psi(x, y, t)$ is a usual wave phase. σ, σ_0 are wave frequencies relative to immovable water at the given and initial time moments $t=t_0$.

The Jacobian function can be written in (2.6) as follows:

$$\frac{\partial(k_x, y)}{\partial(x_0, y_0)} = \frac{\partial k_x}{\partial x} \frac{\partial(x, y)}{\partial(x_0, y_0)} = \frac{\partial k_x}{\partial x} \frac{\partial x}{\partial x_0}. \quad (2.7)$$

Using (2.4) and (2.5) it can be found out that: $\partial k_x / \partial x = -\partial F / \partial x / C_{gx}$; $\partial x / \partial x_0 = C_{gx} / C_{gx0}$. The integral value (2.6) can be estimated with the help of the saddle-point method. The saddle-point k_x^{**} is found using the equation $\partial \Theta / \partial k_x = 0$, where $\Theta(x, k_x) = k_x(x - \tilde{x}) + \tilde{\psi}(x)$.

As soon as $\frac{\partial \Theta}{\partial k_x} = x - \tilde{x} + \left(\frac{\partial \tilde{\psi}}{\partial \tilde{x}} - k_x \right) \frac{\partial k_x}{\partial x} = x - \tilde{x}$, then it turns out that $\tilde{x}(k_x^{**}) = x$ and

$\partial^2 \Theta / \partial k_x^2 = -\partial \tilde{x} / \partial k_x = C_{gx} / (dF/dx)$. An application of the usual saddle-point method to the integral (2.6) leads to the following formula:

$$\eta(x, y, t) = a_0 \sqrt{\frac{\sigma}{\sigma_0} \frac{C_{gx0}}{C_{gx}}} \exp\{i\psi\}. \quad (2.8)$$

The insignificant phase factor is omitted in this ratio. The expression (2.8) makes up a condition of the wave action density preservation.

Now the "turning" point of $x = x^*$ should be considered. A sign of the velocity C_{gx} is changed, and the wave packet propagation begins moving to the opposite direction at this point. In this case: $\partial^2 \Theta / \partial k_x^2|_{k=k^*} = 0$, and the phase expansion $\Theta(k_x)$ starts with the term of order $(k_x - k_x^*)^3$ at the saddle-point $k_x^{**} = k_x^*$:

$$\left. \frac{\partial^3 \Theta}{\partial k_x^3} \right|_{k=x^*} = \frac{\partial}{\partial k} \left(\frac{C_{gx}}{\partial F / \partial x} \right) \Big|_{k=x^*} = \frac{1}{\partial F / \partial x} \frac{\partial C_{gx}}{\partial k_x} \Big|_{k=x^*} \quad (2.9)$$

Considering some area around the turning point $x = x^*$, with the saddle-point k_x^{**} being closed to k_x^* , the expression for $\Theta(k_x)$ can be restricted with the terms of $(k_x - k_x^*)^3$ order. The asymptotic expression can be obtained using such expansion of the integral (2.6) and omitting the insignificant phase factor:

$$\eta(x, y, t) = a_0 \sqrt{2\pi \frac{\sigma}{\sigma_0} \frac{C_{gx}}{\partial F / \partial x}} \kappa^* Ai[\kappa^*(x - x^*)] \exp\{i [k_x^*(x - x^*) + \psi(x^*)]\}, \quad (2.10)$$

Where $Ai(X)$ is the Airy function; $\kappa^* = \left[\frac{1}{2} \frac{1}{\partial F / \partial x} \frac{\partial^2 F}{\partial k_x^2} \right]^{\frac{1}{3}} \Big|_{x=x^*}$.

The Airy function $Ai(X)$ is estimated for the large positive values ($X > 0$) as:

$$Ai \approx \frac{1}{\sqrt{2\pi}} X^{-1/4} \exp\left(-\frac{2}{3} X^{3/2}\right), \quad (2.11a)$$

and for the large negative values ($X < 0$) as:

$$Ai \approx \frac{1}{\sqrt{2\pi}} X^{-1/4} \cos\left(\frac{2}{3}|X|^{3/2} - \frac{\pi}{4}\right). \quad (2.11b)$$

The Airy function can be presented at $X < 0$ as a superposition of two exponential dependencies of the type $\exp(\pm iX)$, one of them describing the straight and the second the reflected waves. These two waves with close wave numbers superimposing each other create the interference pattern, with total amplitude subjected to modulation.

A wave vector component is defined as $k_x = k_x^* \pm \sqrt{\kappa^{*3}(x^* - x)}$ in the vicinity of the turning point.

The (\pm) signs are referred to the straight and reflected waves, respectively. There is a shift by $-\pi/2$ in the reflected wave phase due to the ray touching the caustic. Taking into account the latter ratio in the formula (2.8), as well as applying asymptotic of the Airy function (at $X < 0$) in the formula (2.10), the results are coincided, indicating the uniformity of the asymptotic solution. The solution around the caustic with asymptotic is shown in Fig. 2.3.

The maximum amplitude $a = |\eta|$ is reached with $\kappa^*(x^* - x) = 1.02$; at the same time $Ai = 0.536$.

$$a_{\max} \cong 1.69 a_0 \sqrt{\frac{\sigma}{\sigma_0}} C_{gx} \left| \frac{\partial F}{\partial x} \right|^{\frac{1}{6}} \left(\frac{\partial^2 F}{\partial k_x^2} \right)^{\frac{1}{3}} \Big|_{x=x^*} \quad (2.12)$$

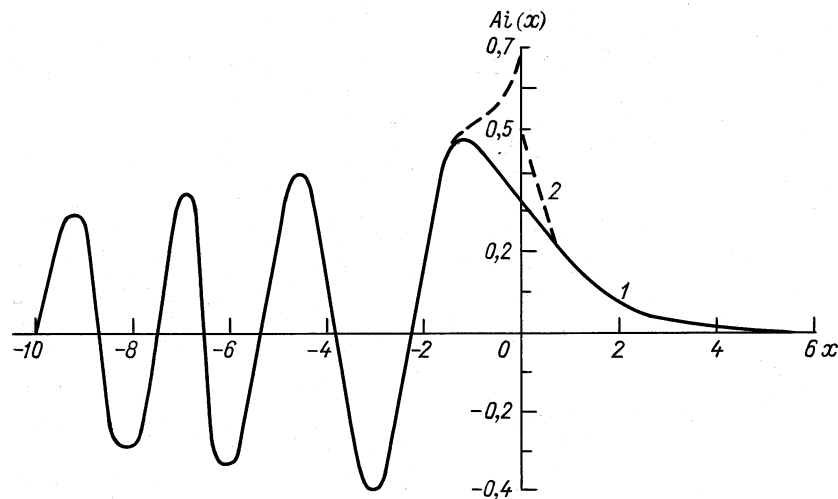


Fig. 2.3. Airy function and its asymptotic approximations (2.11a) for $X > 0$ and (2.11b) for $X < 0$.

$$\frac{\partial F}{\partial x} = k_y \frac{\partial V}{\partial x}; \quad \frac{\partial^2 F}{\partial k_x^2} = \frac{1}{2} \sqrt{g/k^3} \left(1 - \frac{3}{2} k_x^2 k^{-2} \right). \quad (2.13)$$

At the turning point $x = x^*$ the following values are defined as $\kappa_* = \frac{1}{2} \left(\frac{\partial F}{\partial x} \sqrt{\frac{\partial^2 F}{\partial^2 k_x}} \right)^{-1} \Big|_{x=x^*}$,

$C_{gx} = 0$, $k_x = k_x^* = 0$, $\sigma^* / \sigma_0 = \sqrt{k_x / k_0}$. A substitution of these relations to the asymptotic expression (2.6) results in the following free surface elevation:

$$\eta = a_0 \sqrt[3]{4} \sqrt{\pi \cos(\beta_0)} (\sin(\beta_0))^{7/12} \left(\sigma_0 \frac{\partial V}{\partial x} \right)^{1/6} \Big|_{x=x^*} \left(Ai[\kappa_* (x - x^*)] \times \exp[ik_x (x - x^*) + i\psi(x^*)] \right). \quad (2.14)$$

Using this formula it is easy to find out the amplitude maximum, taking place at $\kappa_* (x - x^*) = 1.02$ for the initial angle $\beta_0 = 42.79^\circ$:

$$a_{\max} = 1.04 a_0 \left(\sigma_0 / \frac{\partial V}{\partial x} \right)^{1/6}. \quad (2.15)$$

It should be noted that the expression (2.15) coincides with the earlier derived ratio (Peregrine, 1976), with an exception of using the value $\sigma|_{x=x^*} = \sqrt{gk_y}$ instead of σ_0 . As a result, the amplitude maximum is achieved at $\beta_0 = 45^\circ$, and the numerical coefficient in the expression (2.15) makes up 1.065 (instead of $\beta_0 = \arccos(\sqrt{7/13}) = 42.79^\circ$ and the coefficient of 1.04).

As an example a swell height increase in field condition should be estimated. Thus, if the wavelength is equal to 50 m. and the velocity gradient is $\Delta V / \Delta x = 10^{-4}$, then the swell height increase is equal to ≈ 4.64 .

The wave steepness around the caustic can be easily determined using the expressions (2.3), and (2.15) as:

$$a_{\max} k^* = 1.51 a_0 k_0 (\cos(\beta_0))^{19/12} (\sin(\beta_0))^{1/2} \left(\sigma_0 / \frac{\partial V}{\partial x} \right)^{1/6} \Big|_{x=x^*} \quad (2.16)$$

The maximum of this value is achieved at $\beta_0 = 31.255^\circ$ and it is equal to:

$$(ak)_{\max} = 0.848 a_0 k_0 \left(\sigma_0 / \frac{\partial V}{\partial x} \right)^{1/6} \Big|_{x=x^*} \quad (2.17)$$

Thus, there is strong impact current on wave field around caustic. It can produce amplitude modulation, large wave height amplification up to 4.6, and wave steepness up to 3.8.

3. Non-linear wave interaction in shallow water due to their intersection described by KP equation

Another important current impact on wave evolution is observed, that happens not in a caustic area located at the large current speed gradient, but in the middle part of current where intersection of waves moving from different directions reflected by current (Fig.5). The evolution of this long-wave is described by the Kadomtsev-Petviashvili equation.

Let us consider the reasons in favor of the long-wave shallow water consideration. The data are taken from [2, 3], where it is noted that the ship is lowered down on the long forerunner (or sloping trough) before the rogue wave affects it, see Fig.2. Likely the forerunner is a part of the rogue wave hence one can suggest that the typical horizontal size, L , of the wave lies in the interval $L \approx 500\text{m}$ or the double ship length. The depth of the ocean, H , according to [2, 3] is $H = 200\text{m}$, while the amplitude of the wave, A , is $A = 20\text{m}$. The relationships, $A/H = 0.1$ and $H/L = 0.33$, satisfy the shallow water theory, see, e.g., [10, 12]. Moreover, $A/H = O(H^2/L^2)$, that corresponds to the balance between nonlinearity and dispersion.

Also observations demonstrate us that the rogue wave is a two-dimensional localized or solitary wave. Transverse variation of the horizontal speed of the Agulhas current may be responsible for the transverse localization of the wave. One can see from Fig.2 that typical size of the transverse current variation, Y , is equal to several kilometers. Then the relationship L/Y is of order of H/L , $L/Y = O(H/L)$, and the transverse variations are weaker than those along the current.

Let us consider the ocean as an inviscid liquid layer of permanent depth H while the influence of the open air is negligibly small. Assume the plane $z = 0$ of the Cartesian coordinates coincides with undisturbed free surface of the layer, hence fluid occupies the region $-H < z < q, q(x, y, t)$, is a free surface disturbance. Let us denote the liquid density by ρ , velocity components along axes x, y, z by $u(x, y, z, t)$, $v(x, y, z, t)$ and $\omega(x, y, z, t)$ respectively. Let t is time, p is pressure.

As usual, it is convenient to introduce the velocity potential, $u = \Phi_x$, $v = \Phi_y$ and $\omega = \Phi_z$. Then the governing equations and the boundary conditions are:

$$\Phi_{xx} + \Phi_{yy} + \Phi_{zz} = 0 \quad \text{at } -H < z < q; \quad (3.1)$$

$$\Phi_z = 0 \quad \text{at } z = -H, \quad (3.2)$$

while at $z = q$

$$\rho(\Phi_t + 1/2(\Phi_x^2 + \Phi_y^2 + \Phi_z^2) + gq) = 0 \quad (3.3)$$

$$q_t + \Phi_x q_x + \Phi_y q_y = \Phi_z \quad (3.4)$$

Following the scaling analysis, we shall consider the long waves with small but finite amplitude. Then the scales are introduced as follows: L - for x , Y - for y , H - for z , L/\sqrt{gH} - for t , A - for q , and $AL/H\sqrt{gH}$ - for Φ . The small parameter of the problem, ε , is

$$\varepsilon = A/H = H^2/L^2$$

also it is assumed that $L/Y = \sqrt{\varepsilon}$. Then the asymptotic solution of dimensionless Eq.(3.1) with the boundary condition (3.2) being taken into account, is

$$\Phi = \phi(x, y, t) - \varepsilon \frac{(z+1)^2}{2} \phi_{xx} + \varepsilon^2 \left(\frac{(z+1)^4}{24} \phi_{xxxx} - \frac{(z+1)^2}{2} \phi_{yy} \right) + O(\varepsilon^2), \quad (3.5)$$

Where $\phi(X, y, t)$ is a new unknown function. Substituting (3.5) into the boundary conditions (3.3), (3.4) one can obtain the coupling equations for the functions ϕ and q ,

$$\phi_t + q + \frac{\varepsilon}{2} (\phi_x^2 - \phi_{xxt}) = O(\varepsilon^2) \quad (3.6)$$

$$q_t + \phi_{xx} + \varepsilon((\phi_x q)_x + \phi_{yy} - 1/6\phi_{xxxx}) = O(\varepsilon^2) \quad (3.7)$$

Introducing the phase variable $\theta = x - t$ and the slow time $t = \varepsilon\tau$, one can obtain from the last equations the well known Kadomtsev-Petviashvili (KP) equation [10, 12] for the function $\eta = \phi_\theta$,

$$(2\eta_\tau + 3\eta\eta_\theta + 1/3\eta_{\theta\theta\theta})_\theta + \eta_{yy} = 0 \quad (3.8)$$

It is known that the plane solitary wave solution of Eq.(3.8),

$$\eta = \frac{4k^2}{3} \cosh^{-2} k \left(\theta + my - \frac{3m^2 + k^2}{6} \tau \right), \quad (3.9)$$

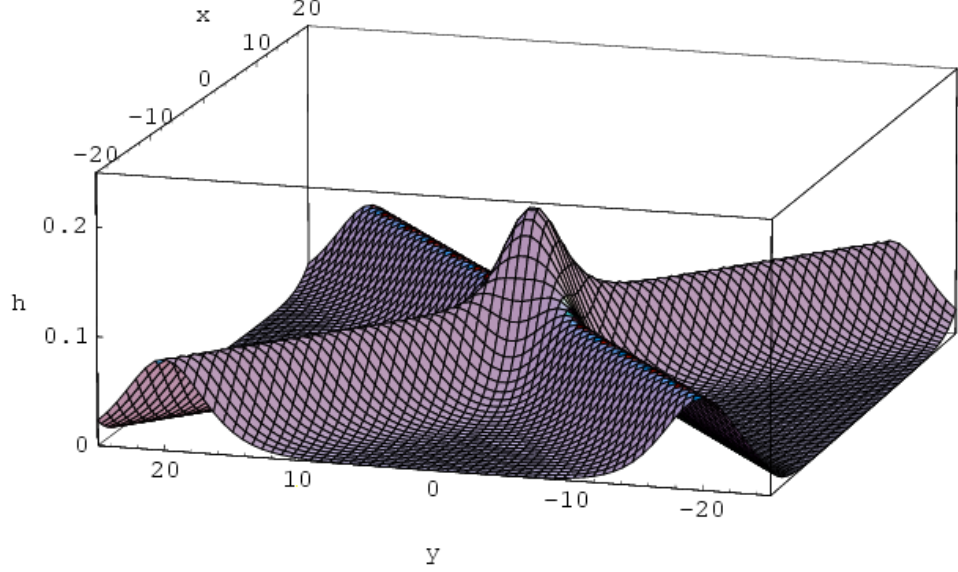


Figure 3.1: Interaction of the plane solitary waves described by the KP two-solitary waves

Solution is stable, and exact two-dimensional localized traveling wave solution requires an opposite sign at η_{yy} or at $\eta_{\theta\theta\theta}$ [10-12]. In our case the negative sign at the dispersion term in Eq. (3.8) may be formally achieved if the surface tension is taken into account. Then the coefficient is changed from $1/3$ to $1/3 - Bo^{-1}$, where Bo is the Bond number. However, its unlikely that the value of the Bond number may be higher than 3 in the ocean.

The KP equation also possesses two-solitary wave solution [10-12],

$$\eta = \frac{4}{3} \frac{\partial^2}{\partial \theta^2} \log(F), F = 1 + \exp(\xi_1) + \exp(\xi_2) + \exp(A_{12} + \xi_1 + \xi_2),$$

$$\xi_i = k_i \left(\theta + m_i y - \frac{3m_i^2 + k_i^2}{6} \tau \right), \exp A_{12} = \frac{(k_1 - k_2)^2 - (m_1 - m_2)^2}{(k_1 + k_2)^2 - (m_1 - m_2)^2} \quad (3.10)$$

Its typical shape is shown in Fig.3.1. One can see a localized structure in the area of the waves interaction. It moves keeping its shape and velocity, but the amplitude is only two times higher than the amplitude of single solitary wave. Recently numerical results on the interactions of two inclined plane solitary waves were performed in Refs.[5]. The initial conditions were used in the form of a linear superposition of the waves (3.9). It was found that the incident waves may be considerably deformed after the interaction. In particular, the initial overlapping part changes its form to a steady two-dimensional localized wave moving along the x -axis. The amplitude of this wave, which is called by stem in [5], is higher than the amplitude of each interacting solitary

waves. The shape of the stem is similar to the localized structure shown in Fig.3.1, however, the possible largest amplitude of the stem wave is four times larger than the amplitude of the incident waves [5]. More important is that the largest amplitude is achieved when the angle between interacting plane solitary waves lies in a certain, rather narrow, interval. In dimensional variables in our case it is equal to 15 - 20 degrees. If the directions of the interacting waves vary, one can suggest the variation of the stem amplitude. If the angle between the waves turns out in the above-mentioned interval near the ship, an abnormally high wave appears suddenly for the crew. However, there is no a forerunner before the stem.

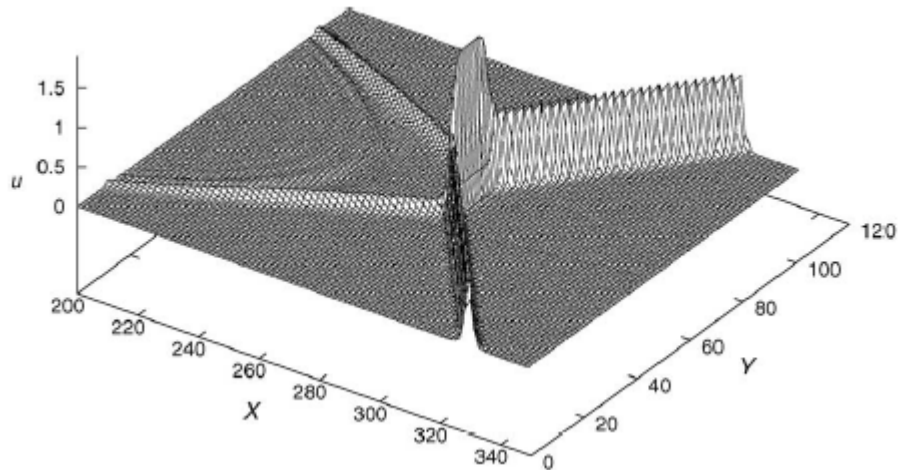


Fig. 3.2 Formation of the stem.

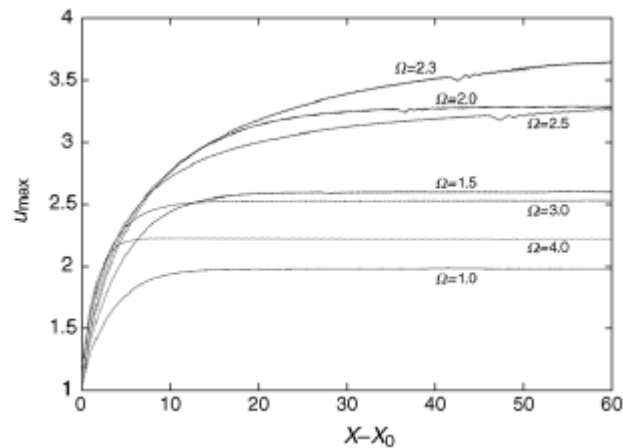


Fig.3.3 Dependence of the stem amplitude on the angle between incident waves.

Much higher amplification of the wave is provided by the interaction of the waves with curved fronts [5], calculations demonstrate an increase in amplitude up to 14 times.

Conclusion

The freak wave generation in spatially non-uniform current may happen due to three main reasons. They can be mentioned as follows:

- Wave energy amplification due to wave-current interaction;
- Wave height amplification around caustic due to refraction wave in non-uniform current;
- Non-linear wave interaction in shallow water due to their intersection described by KP equation;

Acknowledgments

One of the authors (IVL) acknowledges the support of the Russian Foundation for Basic Researches under the grant No 05-05-08027 ofi-a. The authors thank Professor H. Moes for the donation of the data, which is used for preparation of Fig. 3.

References

- [1] M. Olagnon and G.A. Athanassoulis (Eds.), *Rogue Waves-2000*, Ifremer, France, 2001.
- [2] C. Kharif and E. Pelinovsky, Physical mechanisms of the rogue wave phenomenon, *European J. Mechanics/ B - Fluids*, **22** (2003) 603–635.
- Lavrenov I.V., 1985: Ship collision with "freak-wave", *Marine fleet*, **12**, 28—30, in Russian
- [3] I.V. Lavrenov, *Wind Waves in Ocean*, Berlin, Springer, 2003.
- [4] P. Peterson et al., Interaction soliton as a possible model for extreme waves in shallow water, *Nonlinear Processes in Geophysics* **10** (2003) 1–8.
- [5] A.V. Porubov, H. Tsuji, I.V. Lavrenov, and M. Oikawa, Formation of the rogue wave due to nonlinear two-dimensional waves interaction, *Wave Motion*, **42** (2005), No3, 202–210.15
- [6] Maslov V.P., M.V. Fedoryuk, 1976: *Quasi-classical approximation for quantum mechanics equations* (Nauka, Moscow,), in Russian
- [7] Mallory J.K., 1974: Normal waves on the south-east of South Africa, *Inst. Hydrog. Rev.*, **51**, 89—129
- [8] Schuman E.H., 1976: High waves in the Agulhas curren, *Mariners Weather*, Vol.**20**, **1**, 1—5
- [9] H. Moes, Presentation at MaxWave Project Concluding Symposium, Geneva, 8-12 October, 2003.
- [10] M. Ablowitz and H. Segur, *Solitons and inverse scattering transform*, Philadelphia, SIAM, 1981.
- [11] D.E. Pelinovsky and Yu. A. Stepanyants, Solitary Wave Instability in the Positive-Dispersion Media Described by the Two-Dimensional Boussinesq Equations, *JETP* **79** (1994) 105–112.
- [12] B.B. Kadomtsev and V.I. Petviashvili, The stability of solitary waves in a weakly dispersive media, *Sov.Phys.Dokl.* **15**(1970) 539–541 .
- [11] O.M. Philips, *Dynamics of the upper ocean layer*, Cambridge, University Press, 1978.
- [12] Y. Matsuno, Dynamics of interacting algebraic solitons, *Int. J. Mod. Phys. B*, **9** (1995) 1985–2081.
- [13] M.J. Ablowitz and H. Segur, Long internal waves in fluids of great depth, *Stud. Appl. Math.* **62** (1980) 249–262.
- [14] Y. Matsuno, Transverse instability and collapse of internal algebraic solitary waves in fluids of great depth, *Phys. Let. A*, **265** (2000) 358–363.
- [15] G. Whitham, *Linear and Nonlinear Waves*, New York, John Wiley & Sons, 1974.
- 16
- [16] T. Kakutani and N. Yamasaki, Solitary waves on a two-layer fluid, *J. Phys. Soc. Jpn*, **45** (1978) 674–679.
- [17] R. Grimshaw, E. Pelinovsky, and T. Talipova, The modified Korteweg- de Vries equation in the theory of large-amplitude internal waves, *Nonl. Proc. Geophys.*, **4** (1997) 237–250.
- [18] L.A. Ostrovsky and Y.A. Stepanyants, Internal solitons in laboratory experiments: Comparison with theoretical models, *Chaos* **15** (2005) 037111.
- [19] H. Tsuji and M. Oikawa, Oblique interaction of solitary waves in an Extended Kadomtsev-Petviashvili equation. To be published in: *Proceeding of the XXXIII International Conference Advanced Problems in Mechanics*, Saint-Petersburg, Russia, 2005.